Insulator-to-Conducting Transition in Dense Fluid Helium

P. M. Celliers,[1] P. Loubeyre,[2] J. H. Eggert,[1] S. Brygoo,[2] R. S. McWilliams,[3,5] D. G. Hicks,[1] T. R. Boehly,[4] R. Jeanloz,[5] and G. W. Collins[1]

[1]*Lawrence Livermore National Laboratory, Post Office Box 808, Livermore, California 94551, USA*
[2]*CEA/DAM/DIF, 91297 Arpajon. France*
[3]*Institute for Shock Physics, Washington State University, Pullman, Washington 99164, USA*
[4]*Laboratory for Laser Energetics, University of Rochester, Rochester, New York 14623, USA*
[5]*University of California, Berkeley, California 94720, USA*

(Received 12 November 2009; published 5 May 2010)

By combining diamond-anvil-cell and laser-driven shock wave techniques, we produced dense He samples up to 1.5 g/cm^3 at temperatures reaching 60 kK. Optical measurements of reflectivity and temperature show that electronic conduction in He at these conditions is temperature-activated (semiconducting). A fit to the data suggests that the mobility gap closes with increasing density, and that hot dense He becomes metallic above ~1.9 g/cm^3. These data provide a benchmark to test models that describe He ionization at conditions found in astrophysical objects, such as cold white dwarf atmospheres.

DOI: 10.1103/PhysRevLett.104.184503 PACS numbers: 51.50.+v, 52.25.Fi, 62.50.−p, 67.25.bf

Helium is the second most abundant element in the universe, and its properties in the dense high-pressure fluid state are an essential input to model astrophysical objects such as giant planets [1] and white dwarf stars [2]. Of particular interest is the domain on the phase diagram where He makes the transition from an insulator to an electrical conductor. Solid He at low temperature is a wide band-gap insulator [3], with an excitonic level of 21.58 eV. Many calculations have predicted the insulator to conductor transition pressure for solid He with the most recent estimates [4–7] spanning the range 4.4–25 TPa (i.e., 10–21 g/cm^3) much out of reach of static experiments. At elevated temperatures, insulator to conductor transitions have been observed in many wide band-gap insulators, for example, in dense H_2, O_2, and N_2 [8–10] under multishock quasi-isentropic compression, and in Al_2O_3, LiF, H_2O, D_2, SiO_2, and diamond [11–13] under single shock compression. Generally, these transitions occur at lower pressures than the insulator-metal transition of the cold solid. The former three cases have been interpreted in terms of the Mott [14] or Goldhammer-Herzfeld (GH) [15] criteria, i.e., pressure ionization; however, in the case of diamond, the conducting transition is associated with melting, and in the case of single shock-compressed D_2, it is connected with molecular dissociation [12]. Electrical conductivity data has recently been reported in dense fluid He under multiple shock compression [16], in which the conductivity was observed to increase to a value typical of liquid alkali metals. The density of the metallic-like state (not directly inferred) was estimated from hydrodynamic calculations to be around 1 g/cm^3 [17]. However, this value of the density is surprisingly much smaller than the insulator-metal density predicted by the GH criterion (~7.7 g/cm^3) or by the Mott criterion (~4.7 g/cm^3). Recently, various theoretical calculations [5,7,18] have reached conclusions indicating that around 1 g/cm^3, the conductivity of dense fluid He should be temperature activated or semiconducting.

In a previous Letter [19], we reported Hugoniot data for He by laser shock compression, obtained at the OMEGA laser facility. The samples were statically precompressed in diamond-anvil cells to produce Hugoniot measurements (i.e., of the shock-compressed density ρ and pressure P) for shocks incident on samples of various initial densities, ρ_0 (spanning the range from the cryogenic liquid density $\rho_{0L} = 0.123$ g/cm^3 to $3.3\rho_{0L}$). Here, we report on measurements of temperature T and of reflectivity R at 532 nm that were performed simultaneously with the Hugoniot measurements. The reflectivity measurements were obtained from velocity interferometer [20] data at the operating wavelength of the probe laser (532 nm). Simultaneously, temperature was inferred from a streaked optical single-channel pyrometer [21] which images the thermal emission of the shocked sample over a wavelength band centered at 650 nm with a 100 nm bandwidth. The temperature is then determined using the grey body approximation (Planck spectrum), assuming a wavelength-independent emissivity, given by $(1 - R)$ with R being the measured optical reflectivity at 532 nm [22].

In Fig. 1(a), the temperature data are plotted against pressure along two Hugoniot curves centered on the initial densities ρ_{0L} and $3.3\rho_{0L}$, corresponding to initial sample pressures, respectively, of 0.12 and 1.25 GPa. The much lower temperatures observed along the $3.3\rho_{0L}$ Hugoniot curve illustrates how precompressed samples can be used to create shock states that are denser and cooler than those produced with cryogenic samples. A detailed comparison between experimental data and calculations is shown for the Hugoniot curve centered on ρ_{0L}. The measured peak compression ratio of 6 is in good agreement with the

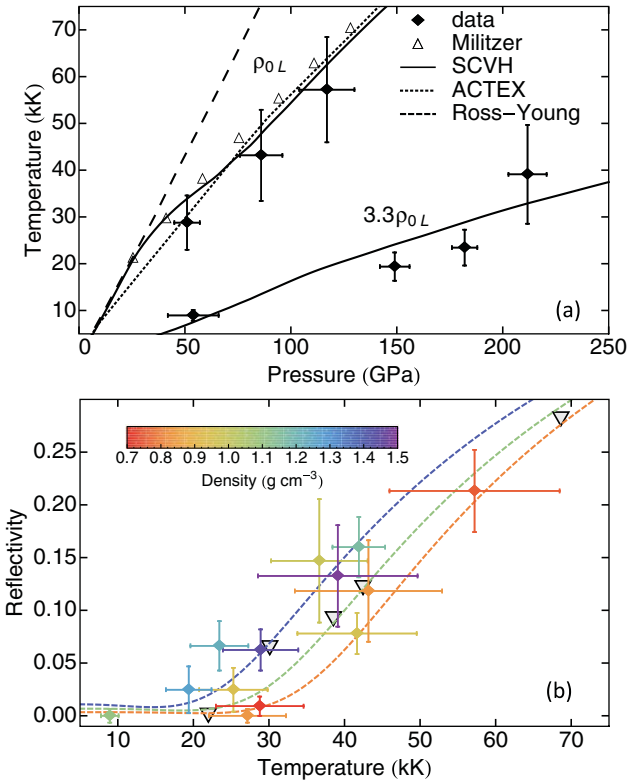

FIG. 1 (color). (a) Variation of observed temperature versus Hugoniot pressure for two Hugoniots centered at $\rho_{0L} = 0.123$ g/cm^3 and $3.3\rho_{0L}$, where ρ_{0L} is the cryogenic liquid density. Also shown are the temperatures predicted by several models for the ρ_{0L} initial density: PIMC [25], ACTEX [24], SCVH [23], and Ross and Young [24,27]. (b) Solid diamonds show the observed reflectivity as a function of temperature and final density indicated by the color scale. Curves show the reflectivity obtained from a fit to the data using the semiconductor Drude model for three final state densities: 0.8, 1.1, and 1.4 g/cm^3. Gray triangles are calculated reflectivities by Kowalski *et al.* [5] near 1 g/cm^3 with a +3 eV gap correction.

astrophysical EOS of Saumon, Chabrier, and van Horn (SCVH) [23] and the ACTEX model [24], but slightly larger than recent *ab initio* predictions [25]. Very recently, a study of the quartz Hugoniot curve [26] (relevant to the impedance-matching analysis) suggests that a stiffer model for the quartz compressibility should be used to analyze the data; for the present study, we use the densities reported in [19] and estimate that the new calibration will shift the densities lower by about 10% [22]. The Ross and Young soft sphere model [24,27] does not include electronic excitations and predicts higher temperatures than experiment with a peak compression of only 4. Electronic excited and ionized states are taken into account by the SCVH, ACTEX, and *ab initio* calculations and constrain the temperature rise along the Hugoniot curve, in good agreement with experiment. From the temperature data the maximum compression of 5–6 on the He Hugoniot curve centered at the initial density ρ_{0L} occurs at about 100 GPa and 55 000 K (55 kK). While the temperature data are not accurate enough to discriminate among models, optical reflectivity is a more suitable probe.

The reflectivity data of He along the Hugoniot curves for various initial densities are plotted versus temperature in Fig. 1(b). Within the range of final state densities obtained in our experiments (0.7–1.5 g/cm^3), the rise of reflectivity in He is connected with the increasing ionization and exhibits a strong temperature dependence along with a density dependence. While the reflectivity increases monotonically with temperature for all final state densities, the threshold for onset of measurable reflectivity shifts to *lower* temperatures with increasing final state density. At a density around 0.8 ± 0.2 g/cm^3, reflectivity above our detection limit (about 2%) occurs above a temperature threshold of about 30 kK, while at 1.3 ± 0.2 g/cm^3, observable reflectivity occurs above temperatures around 21 kK. *Ab initio* calculations using density functional theory (DFT) and the Kubo-Greenwood formulation have shown that the optical conductivity of He has a Drude-like behavior for photon energies below 10 eV at the thermodynamic conditions of the present study [5,18]. A DFT calculation of reflectivity with a +3 eV correction to the electronic gap, shown in Fig. 1(b), compares well with the experimental data [5], indicating the data are consistent with a gap energy around 10 eV.

Curves shown in Fig. 1(b) show the density dependence of the reflectivity as predicted by a simple semiconducting Drude model that has been fitted to our data. We have applied a variation on this model to shock front reflectivity data of other wide-band-gap materials: water [11], Al_2O_3, and LiF [13]. Subsequent independent DFT modeling of the shocked LiF case found the simple semiconducting Drude picture to provide an accurate representation of the detailed results [28]. The reflectivity data can be related to the optical conductivity $\sigma(\omega)$ through the complex index of refraction $n = [\varepsilon_b + i\sigma(\omega)/\omega]^{1/2}$, where ε_b is the contribution of the bound electrons, estimated from experimental refractive index data [29]. For the shock front in the precompressed sample, the Fresnel reflectivity is given by $R = |(n - n_0)/(n + n_0)|^2$, where n_0 is the index of the precompressed sample in its initial state [30]. Applying the Drude model for the conductivity, $\sigma(\omega) = (n_e e^2 \tau/2m_{\text{eff}})(1 - i\omega\tau)^{-1}$, the reflectivity is expressed as a function of the electron relaxation time, τ, and carrier concentration, n_e; here, $m_{\text{eff}} = \gamma m_e$ is the electron effective mass expressed in terms of the vacuum mass m_e and a fitting parameter γ. The temperature-activated carrier concentration is given by the model for an intrinsic semiconductor $n_e = 2(m_{\text{eff}} kT/2\pi\hbar^2)^{3/2} f_{1/2}(-E_g/(2kT))$, where $f_m(x) = (2/\sqrt{\pi}) \int_0^\infty y^m/(1 + e^{y-x}) dy$ is the Fermi-Dirac integral and E_g is the gap energy. For E_g, we assumed initially a density and temperature dependent formula: $E_g = E_0 - A(\rho/\rho_{0L}) + B(T/T_0)$, where $kT_0 = 24.6$ eV.

We fit the modeled reflectivity $R_M(n_0, \rho, T)$ to match the observed R using orthogonal distance regression [31]. The data are insufficient to constrain E_0, A, B, and γ simultaneously, and the fit is least sensitive to the temperature coefficient B [32]. Therefore, we set $B = 0$, and find the best fit (spanning a range of densities from 0.7 to 1.5 g/cm^3) gives $A = 1.34 \pm 0.28$, $E_0 = 20.4 \pm 3.7$ eV, $\gamma = 0.62 \pm 0.17$. The linear density dependence of the gap function, shown in Fig. 2(a), gives $E_g = 20.4$ eV at $\rho = 0$, comparable to the 24.6 eV ionization energy of the isolated atom, and to the 21.6 eV excitonic gap in solid He at 0.2 GPa and 0.18 g/cm^3 [3]. At higher densities, the fit extrapolates to $E_g = 0$ at a density of $\rho \sim 1.9$ g/cm^3 suggesting gap closure and metallization of the disordered fluid near this density for temperatures below 30 kK. In the middle of the range of our measurements, near 1 g/cm^3, the gap energy is ~10 eV, significantly larger than the temperatures reached in our measurements, and consistent with the use of a semiconducting model. The gap energy near 1 g/cm^3 agrees well the predictions of [5,7] although the density dependence is much steeper.

In Fig. 2(b), $\sigma_{DC}(\rho, T)$ as extracted from the fitted Drude model is plotted versus density with colors indicating temperature. The conversion of the reflectivity data to conductivity data is insensitive to the uncertainties of the various parameters of our fit. The detection limit for reflectivity, about 2%, corresponds to conductivities above $\sim 2.5 \times 10^4$ $(\Omega\,\mathrm{m})^{-1}$. Compared to two DFT calculations [5,18], the estimated Drude conductivities from the present data are in reasonably good agreement. However, they have a different slope for a given isotherm, a consequence of the weaker density dependence of the gap energy in those models. The conductivity data of Ternovoi *et al.* [16] exhibit a rapid rise of conductivity at *estimated* densities around 1 g/cm^3, which led to the interpretation of pressure ionization. Those conductivities are comparable to our measurements, and the density dependence appears close to the slope of the 17 kK isotherm of our fit, similar to the estimated peak temperatures of that experiment. This suggests that our data and fit are consistent with Ternovoi data set, if their densities are increased by about 25%.

The phase diagram of He on the density-temperature plane is sketched in Fig. 3 for densities from 0.2–10 g/cm^3. While the solid is expected to remain insulating, the dense fluid phase has been predicted to exhibit an insulator-to-conductor transition. The present density–temperature data are plotted with a color scale mapped to conductivity. Below 1 g/cm^3, the conductivity is temperature activated with gap energy >10 eV. Under these conditions, the ionization is relatively weak: at $\rho = 1$ g/cm^3 and $T = 20$ and 50 kK, the ionization states estimated from the Drude-semiconducting model fit are 0.6% and 11%, respectively. The density dependence evident in the data produces the curvature of the conductivity contours, indicating that at densities approaching 2 g/cm^3, metallization

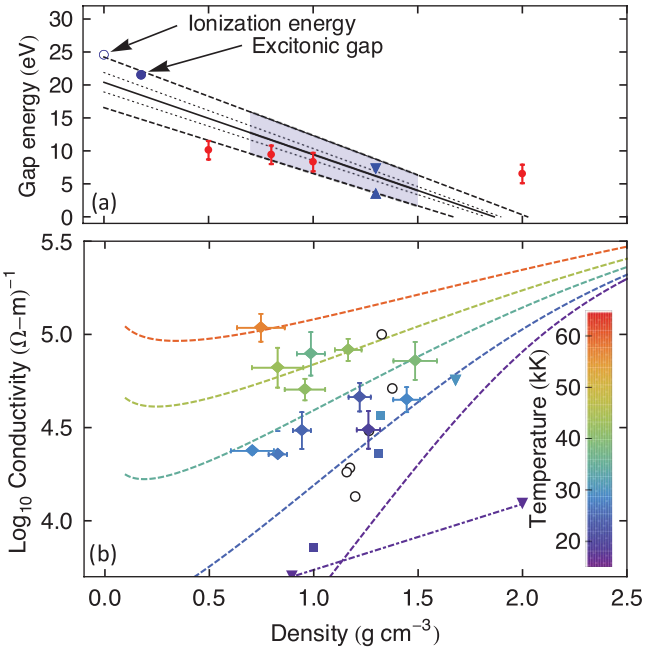

FIG. 2 (color). (a) Energy gap as a function of density (solid curve) as determined from the best fit to the reflectivity data along with the 68% joint-parameter confidence band for the fit (dashed curves). The shaded region spans the density range of our measurements. The dotted curves show the gap function obtained when the parameter B is set to +20 and −20, respectively. Solid (red) circles with error bars show the gap calculated by Kowalski *et al.* [5] at $T = 3$ eV; solid (blue) triangles show the gap calculated by Stixrude and Jeanloz [7] at $T = 1.7$ eV (inverted) and $T = 4.3$ eV (upright). Annotations indicate the ionization energy of the isolated atom and the excitonic gap of solid He at 0.2 GPa [3]. (b) Solid diamond symbols show the DC conductivity inferred from the reflectivity; dashed curves show the conductivity extracted from the semiconductor Drude fit to the reflectivity data at 17, 25, 35, 45, and 60 kK. Colors indicate temperature (inset scale). Other symbols show DC conductivities as follows: solid squares calculated by Kietzmann *et al.* [18]; solid inverted triangles calculated by Kowalski *et al.* [5]; open circles show the data set collected by Ternovoi *et al.* [16] (temperatures not reported). The dot-dash line connects a pair of calculations at 17.4 kK by Kowalski *et al.* to show the density dependence.

(gap closure) should be achieved. This dependence probably applies only to the fluid phase, as the solid phase at similar densities is expected to remain insulating (as is the case for diamond and SiO_2).

Two chemical models have predicted abrupt density induced ionization mechanisms. The first model [33] predicted a first order transition from He to He^+ near 5 g/cm^3, and a later calculation [34] predicted a direct transition from He to He^{+2} near 10 g/cm^3, indicated in Fig. 3. While the location (or existence) of these transitions is debatable, our data cannot rule them out. An interesting experimental domain would be to look at the ionization in the 2–4 g/cm^3 density range below 10 kK. This regime can be accessed

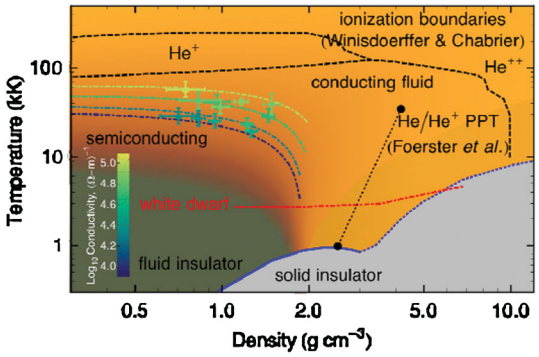

FIG. 3 (color). Phase diagram of He showing the data set (solid diamond symbols) obtained from the precompressed samples along with contours (dash-dot curves) of 4 levels of conductivity: 1, 2, 5, and 10×10^4 $(\Omega - \mathrm{m})^{-1}$. Colors of the symbols and dash-dot curves indicate the DC conductivity (inset scale). Ionization boundaries (black line) of two chemical models are from Foerster *et al.* [33] (dotted line) and Winisdoerffer and Chabrier. [34] (dashed line). The melt curve (blue) is an extrapolation of a Ketchin fit to experimental data [37] (solid line) and extrapolated to higher densities along a path similar to Ref. [33] (dotted line). The temperature-density profile of the WD star is from [2].

with initial pressures in the range of 6–10 GPa, and drive laser energies ≥ 10 kJ.

The present data are relevant for modeling the opacity of white dwarf (WD) stars. The large surface gravity of white dwarfs causes stratifications leading to nearly pure hydrogen and He atmospheres. The pure He atmospheres have lower opacities and so the fastest cooling rate [35]. An accurate model of He white dwarf cooling is thus greatly influenced by the treatment of the ionization of He in the warm dense regime. In Fig. 3, we have indicated the density–temperature profile of an He-rich WD [2]. The extension of the present measurements to 2–4 $\mathrm{g/cm^3}$ will reveal how and where He ionizes within the WD atmosphere. The importance of such knowledge for cosmochronology has been extensively discussed in the literature [36]. The present data already suggest that the He layer is significantly more opaque than previously estimated.

We thank the reviewers for helpful comments and the OMEGA operations staff for their invaluable assistance, M. Millerioux (CEA) for doing the diamond coating, and W. Unites (LLNL) for preparing the quartz plates. This work was performed under the auspices of the U.S. Department of Energy by Lawrence Livermore National Laboratory under Contract No. DE-AC52-07NA27344.

[1] J. J. Fortney, Science **305**, 1414 (2004).
[2] P. Bergeron, D. Saumon, and F. Wesemael, Astrophys. J. **443**, 764 (1995).
[3] R. LeToullec, P. Loubeyre, and J. P. Pinceaux, Phys. Rev. B **40**, 2368 (1989).
[4] S. A. Khairallah and B. Militzer, Phys. Rev. Lett. **101**, 106407 (2008).
[5] P. M. Kowalski *et al.*, Phys. Rev. B **76**, 075112 (2007).
[6] G. Reinisch, J. de Freitas Pacheco, and P. Valiron, Phys. Rev. A **63**, 042505 (2001).
[7] L. Stixrude and R. Jeanloz, Proc. Natl. Acad. Sci. U.S.A. **105**, 11071 (2008).
[8] S. T. Weir, A. C. Mitchell, and W. J. Nellis, Phys. Rev. Lett. **76**, 1860 (1996).
[9] R. Chau *et al.*, Phys. Rev. Lett. **90**, 245501 (2003).
[10] M. Bastea, A. C. Mitchell, and W. J. Nellis, Phys. Rev. Lett. **86**, 3108 (2001).
[11] P. M. Celliers *et al.*, Phys. Plasmas **11**, L41 (2004).
[12] P. M. Celliers *et al.*, Phys. Rev. Lett. **84**, 5564 (2000).
[13] D. G. Hicks *et al.*, Phys. Rev. Lett. **91**, 035502 (2003).
[14] N. F. Mott, *Metal-Insulator Transitions* (Taylor and Francis, London, 1974).
[15] K. F. Herzfeld, Phys. Rev. **29**, 701 (1927).
[16] V. Y. Ternovoi *et al.*, in *Shock Compression of Condensed Matter, 2001*, edited by M. D. Furnish, N. N. Thadhani, and Y. Horie, AIP Conf. Proc. No. 620 (AIP, New York, 2002), 107.
[17] V. E. Fortov *et al.*, JETP **97**, 259 (2003).
[18] A. Kietzmann *et al.*, Phys. Rev. Lett. **98**, 190602 (2007).
[19] J. Eggert*et al.*, Phys. Rev. Lett. **100**, 124503 (2008).
[20] P. M. Celliers *et al.*, Rev. Sci. Instrum. **75**, 4916 (2004).
[21] J. E. Miller *et al.*, Rev. Sci. Instrum. **78**, 034903 (2007).
[22] See supplementary material at http://link.aps.org/supplemental/10.1103/PhysRevLett.104.184503 for details of the analysis methods.
[23] D. Saumon, G. Chabrier, and H. M. van Horn, Astrophys. J. Suppl. Ser. **99**, 713 (1995).
[24] M. Ross *et al.*, Phys. Rev. B **76**, 020502 (2007).
[25] B. Militzer, Phys. Rev. Lett. **97**, 175501 (2006).
[26] M. D. Knudson and M. P. Desjarlais, Phys. Rev. Lett. **103**, 225501 (2009).
[27] M. Ross and D. A. Young, Phys. Lett. A **118**, 463 (1986).
[28] J. Clerouin *et al.*, Phys. Rev. B **72**, 155122 (2005).
[29] A. Dewaele *et al.*, Phys. Rev. B **67**, 094112 (2003).
[30] The shock front Fresnel reflectivity assuming compression only (<0.007) cannot account for the observed reflectivities.
[31] P. T. Boggs, R. H. Byrd, and R. B. Schnabel, SIAM J. Sci. Stat. Comput. **8**, 1052 (1987).
[32] To estimate the range of plausible values for B, we have tested permutations where one of the other parameters are fixed and find $B = 0 \pm 20$ (see Fig. 3).
[33] A. Foerster, T. Kahlbaum, and W. Ebeling, Laser Part. Beams **10**, 253 (1992).
[34] C. Winisdoerffer and G. Chabrier, Phys. Rev. E **71**, 026402 (2005).
[35] C. A. Iglesias, F. J. Rogers, and D. Saumon, Astrophys. J. **569**, L111 (2002).
[36] G. Fontaine, P. Brassard, and P. Bergeron, Publ. Astron. Soc. Pac. **113**, 409 (2001).
[37] F. Datchi, P. Loubeyre, and R. LeToullec, Phys. Rev. B **61**, 6535 (2000).